第 44 卷 第 1 期/2024 年 1 月/光学学报 特邀论文

光学学报

深海级分布式光纤地震系统的南海海试

邓棣珉[1]，徐团伟[1,2*]，张汉羽[3**]，于春亮[4]，曹凯[1,2]，姜英豪[1,2]，谢亚宁[1,2]，李芳[1,2]，吴时国[3]

[1]中国科学院半导体研究所传感技术国家重点实验室，北京 100083；

[2]中国科学院大学材料科学与光电技术学院，北京 100049；

[3]中国科学院深海科学与工程研究所深海地球物理与资源研究室，海南 三亚 572000；

[4]中国科学院深海科学与工程研究所深海工程技术部，海南 三亚 572000

摘要 分布式光纤声传感(DAS)技术将单根光纤视为传感和传输介质，可实时探测光纤附近的振动/声波信号，具有环境适应性强、长距离、空间连续测量等优势。本文借助海底观测平台，将DAS解调仪与传感光纤一同布放于深海，展开了为期21天的深海原位测试试验。在1423 m的深海环境中，成功实现海底振动传感系统，其平均背景噪声约为0.464 mrad/$\sqrt{\text{Hz}}$。这一结果与实验室测量结果相近。海试的数据采集结果进一步验证了该系统的可行性，通过对不同工作状态(入水、着底、移动和抛载上浮)下采集到的振动信号的时频特性进行了分析，能够清晰识别出各工作状态下的信号特征。该深海级分布式光纤地震系统提供了一种新的工程方案，海底的原位布放可以实现在更远海域和更深海底的分布式光纤地震采集，对海洋地球物理研究具有重要意义。

关键词 海底分布式光纤地震系统；分布式光纤声传感；海洋环境监测；海洋地球物理

中图分类号 P315.62；TP212.14 **文献标志码** A **DOI**：10.3788/AOS231425

1 引 言

分布式光纤声传感(DAS)技术通过将传感光纤的一端接入解调仪，注入探测激光脉冲并接收由光纤内部杂质引起的相干背向散射信号，并对固定标距(GL)间隔的瑞利信号相位差进行相位解调获取沿光纤的应变或应变率信息，从而将传感光纤转化为一条紧密排布的声波传感器阵列[1]。DAS具有长距离、高灵敏度、高空间分辨率、抗电磁干扰、无源、低成本等特点，与传统光纤水听器(FOH)阵列不同的是，DAS系统仅由一根光纤和解调仪组成，极大精简了传感部件，该技术为海洋水声传感提供了崭新的发展方向。DAS技术近年来发展迅猛，包括高稳光源[2-4]、脉冲调制[5-8]、外置放大[9-12]、解调算法[13-17]以及信号识别[18-20]等多方面的技术革新，大大提升了其性能和适用范围，使其在油气勘探及海洋研究等领域的应用取得了显著的进展。DAS技术得以高速发展，最早是由于其在油气勘探领域的应用示范和巨大价值。2011年，荷兰壳牌公司Mestayer等[21]首次报道了DAS用于陆上垂直地震测井(VSP)的外场试验结果。2013年，挪威国家石油公司Madsen等[22]报道了利用DAS在北海Gulltopp油田利用海上油井进行VSP测试。海洋环境为DAS技术发展提供了机遇和挑战，近乎恒定温度的环境为极低频地震波探测提供了良好条件。2019年，Lindsey等[23]利用沿加利福尼亚州近海大陆架的科学光缆开展DAS实验，获得了微地震波场的记录。同年，Sladen等[24]和Williams等[25]通过将现有的海底通信光缆连接到DAS，探测到海洋微地震噪声和海浪信号。此后，Spica等[26]、Cheng等[27]和Williams等[28]利用海底光缆监测海洋环境噪声，并通过被动噪声方法对浅海底沉积物的结构进行成像。另一方面，Matsumoto等[29]和Taweesintananon等[30]利用基于气泡震源激发的主动源方法获得了近地表海底沉积物的横波速度结构。Rivet等利用DAS系统进行海上交通监测，而Bouffaut等在北极探测到了须鲸的活动信号[31-32]。

目前海上的DAS应用通常仅在岸上接入海底光缆，尽管DAS方法具有较高的灵敏度和分辨率，但受限于激光光源，目前仅能实现百公里量级的分布式声波传感。因此，难以将其应用于洲际海底长拖通信光缆。本文介绍了一种结合水下试验观测站的DAS海底原位监测系统，该系统主要由深渊耐压舱与DAS解调仪组成，并且通过了110 Mpa的模拟打压测试，可满

收稿日期：2023-08-16；**修回日期**：2023-09-27；**录用日期**：2023-10-26；**网络首发日期**：2023-11-05

基金项目：国家重点研发计划(2023YFC3010700)、崖州湾科技城科研项目(SKJC-2020-01-009)、中国科学院先导专项(XDA22040105)；

通信作者：*xutuanwei@semi.ac.cn；**zhanghy@idsse.ac.cn

足在万米深渊的工作要求。本文首先介绍了该DAS系统的技术原理，然后阐述了其系统设计，最后介绍了1423 m的DAS深海海试，并对深海/深渊基站不同工作状态（入水、着底、移动和抛载上浮）下的时频域特性进行了分析。

2　深海分布式光纤地震系统

深海DAS系统总体由仪器舱支架、仪器舱体、光缆盒组成。仪器舱支架主要用于固定深海DAS系统仪器舱并将其安装在深海/深渊基站上，仪器舱端盖上通过水下光缆穿舱件将传感光纤引出到位于支架底部的光缆盒，光缆盒内盘绕了约600 m的光缆。图1为深海DAS系统示意图。

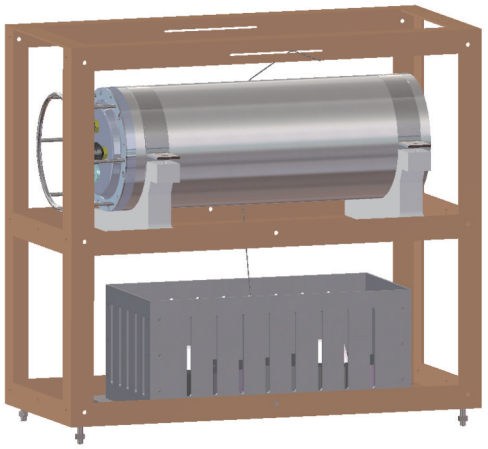

图1　深海DAS系统示意图

Fig. 1　Diagram of deep sea DAS system

2.1　相位载波生成解调算法

小型化DAS模块被封装在仪器舱内，DAS模块包括光电集成单元和数据处理单元，其中光电集成单元与传感光缆连接，而数据处理单元为其提供驱动信号和载波信号。该DAS模块采用相位产生载波（PGC）解调算法，并进行了低功耗光电设计，最低可至25 W，且其大小也仅为150 mm×300 mm×110 mm（宽×深×高）。

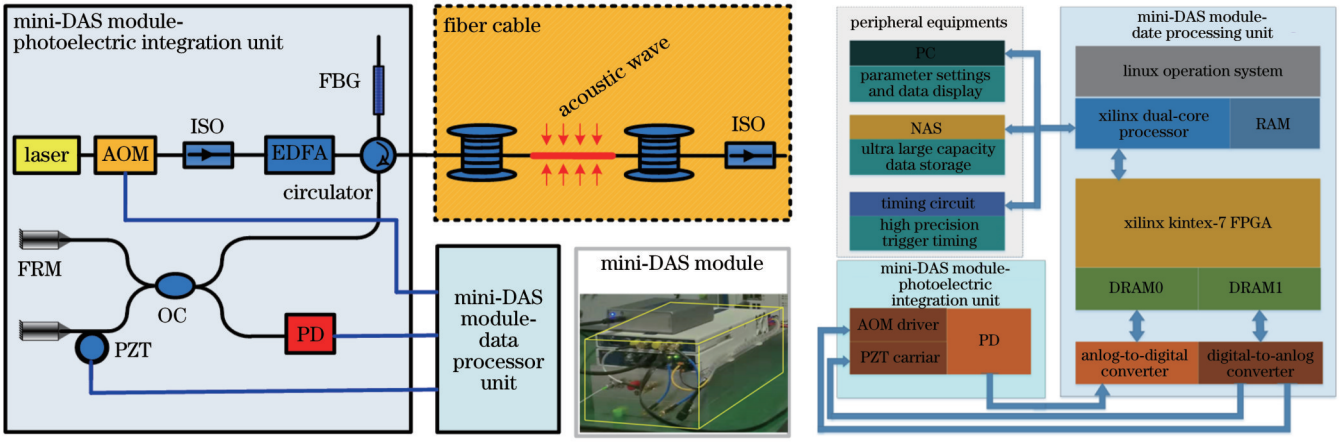

AOM: acousto-optic modulator; ISO: isolator; FBG: fiber Bragg grating; FRM: Faraday rotating mirror; PZT: piezoelectric ceramics; OC: optical coupler; PD: photodetector; NAS: network attached storage; FPGA: field-programmable gate array; RAM: random access memory; DRAM: dynamic random access memory

图2　小型化DAS模块的光路结构与硬件组成

Fig. 2　Structure and data processing frame of mini-DAS module

图2是小型化DAS模块的光路结构和硬件组成示意图，小型化DAS模块通过使用非等臂的迈克尔逊干涉仪（MI）来实现PGC解调算法，以解决偏振衰落问题。MI的输出信号可以表示为

$$I=A+B\cos\left[C\cos\omega_0 t+\varphi(t)\right],\tag{1}$$

式中：$C\cos\omega_0 t$与施加到压电陶瓷（PZT）上的载波信号成正比；$\varphi(t)$是待测的相位变化。然后对式（1）进行贝塞尔展开，如下所示：

$$I=A+B\left\{\left[J_0(C)+2\sum_{k=1}^{\infty}(-1)^k J_{2k}(C)\cos 2k\omega_0 t\right]\cos\varphi(t)-2\left[\sum_{k=0}^{\infty}J_{2k+1}(C)\cos(2k+1)\omega_0 t\right]\sin\varphi(t)\right\}。\tag{2}$$

将干涉信号$I(t)$拆分，并与PGC信号的基频载波和二次谐波载波，即$\cos(\omega_0 t)$和$\cos(2\omega_0 t)$相乘，生成两个多项式，如下所示：

$$BJ_0(C)\cos\omega_0 t\cos\varphi(t)+B\sum_{k=1}^{\infty}(-1)^k J_{2k}(C)\left[\cos(2k+1)\omega_0 t+\cos(2k-1)\omega_0 t\right]\cos\varphi(t)-$$

$$B\sum_{k=0}^{\infty}(-1)^k J_{2k+1}(C)\left[\cos(2k+1)\omega_0 t+\cos 2k\omega_0 t\right]\sin\varphi(t),\tag{3}$$

$$B\cos 2\omega_0 t+BJ_0(C)\cos 2\omega_0 t\cos\varphi(t)+B\sum_{k=1}^{\infty}(-1)^k J_{2k}(C)[\cos(2k+2)\omega_0 t+\cos(2k-2)\omega_0 t]\cos\varphi(t)-$$
$$B\sum_{k=0}^{\infty}(-1)^k J_{2k+1}(C)[\cos(2k+3)\omega_0 t+\cos(2k-1)\omega_0 t]\sin\varphi(t)。\tag{4}$$

然后，将它们通过低通滤波器进行处理，这些滤波器的截止频率应小于PGC信号频率的一半，以消除高频干扰。处理后的信号是平行分量$I(t)$和正交分量$Q(t)$，可以表示为

$$\begin{cases} I(t)=-BJ_1(C)\sin\varphi(t) \\ Q(t)=-BJ_2(C)\cos\varphi(t) \end{cases},\tag{5}$$

式中，$J_1(C)$和$J_2(C)$分别是第一类贝塞尔函数的一阶和二阶。如果调整C的值以确保$J_1(C)=J_2(C)$，则C的值将为2.63。为了计算相位，将采用反正切算法：

$$\varphi(t)=\mathrm{arctg}\left[\frac{I(t)}{Q(t)}\right],\tag{6}$$

式中，$\varphi(t)$是与外界扰动相关的相位变化。表1列出了PGC-DAS系统的具体技术指标。

表1　PGC-DAS系统技术指标

Table 1　Specifications of PGC-DAS system

Instrument noise /(pε/$\sqrt{\text{Hz}}$@10 m)	≤12
SNR /(dB@10 Hz)	≥60
Frequency range /Hz	1—500
Distance /km	≥10
Space resolution /m	10

2.2　深渊仪器舱

小型化PGC-DAS模块被封装于仪器舱内。该仪器舱采用适用于深海环境的钛合金材料，具有高强度、低密度和耐腐蚀的特性，能够承受全海深的超高水压。仪器舱通过110 Mpa水压下的静力学仿真测试和实地耐压测试，表明设备可以在11000 m深渊层的水压下正常工作。仪器舱的内部支架上安装了系统电源模块、控制模块、冷却风扇和小型化DAS模块等设备。仪器舱的端盖上配备了供电接口、通信接口以及光缆穿舱接口。图3为相关结构图。

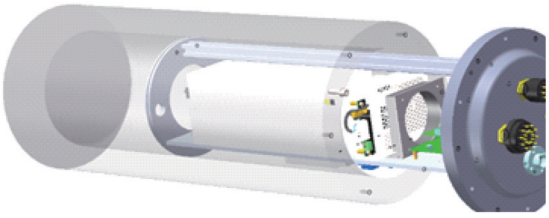

图3　深渊仪器舱结构图

Fig. 3　Structure diagram of pressure chamber for abyss

3　基站工作状态监测

2022年5—6月，深海DAS系统搭载深海/深渊原位科学实验站（以下简称：基站），在中国南海海域进行了为期21天的深海测试（见图4）。深海/深渊基站是用于海底原位调查的实验平台，具备自动浮潜以及海底位点转移的能力。本次海试目的之一是验证该DAS系统在深海环境作业的可靠性和稳定性，以及长时间的地震数据采集能力。本文介绍了深海DAS对作业流程中基站状态的监测结果，包括侧重分析深海/深渊基站不同工作状态（入水、着地、移动和抛载上浮）下的结果。

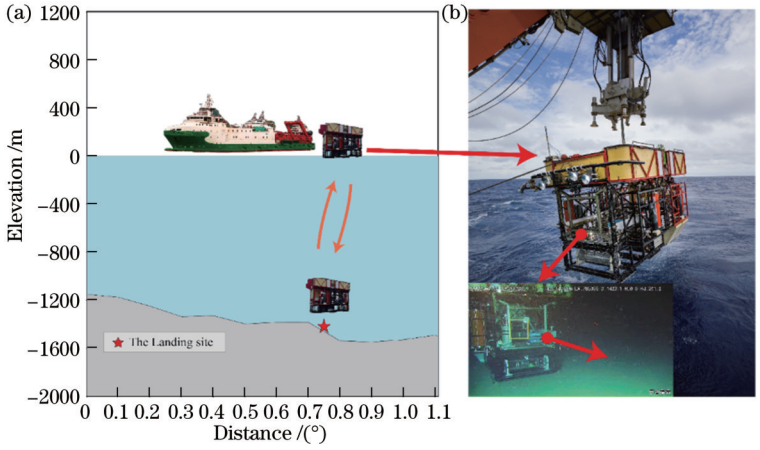

图4　海试现场示意图。(a)海试位置的地形图；(b)基站的实验状态图

Fig. 4　Picture of sea trial. (a) Topographic map of location of sea trail; (b) photos of experimental site

图5揭示了基站进入水面的过程。图5(a)为时长60 s的DAS数据瀑布图，记录了基站与水面碰撞产生振动的整个过程。图5(b)和5(c)分别是基站入水的第57道数据记录及其时频谱，从中可以看出，在第20

s处记录到一个较强的宽带信号，对应于基站底部与海面首次接触产生的振动。随后基站的其余模块依次进入水中，并与水面发生局部碰撞，产生了一系列相对较弱的振动。

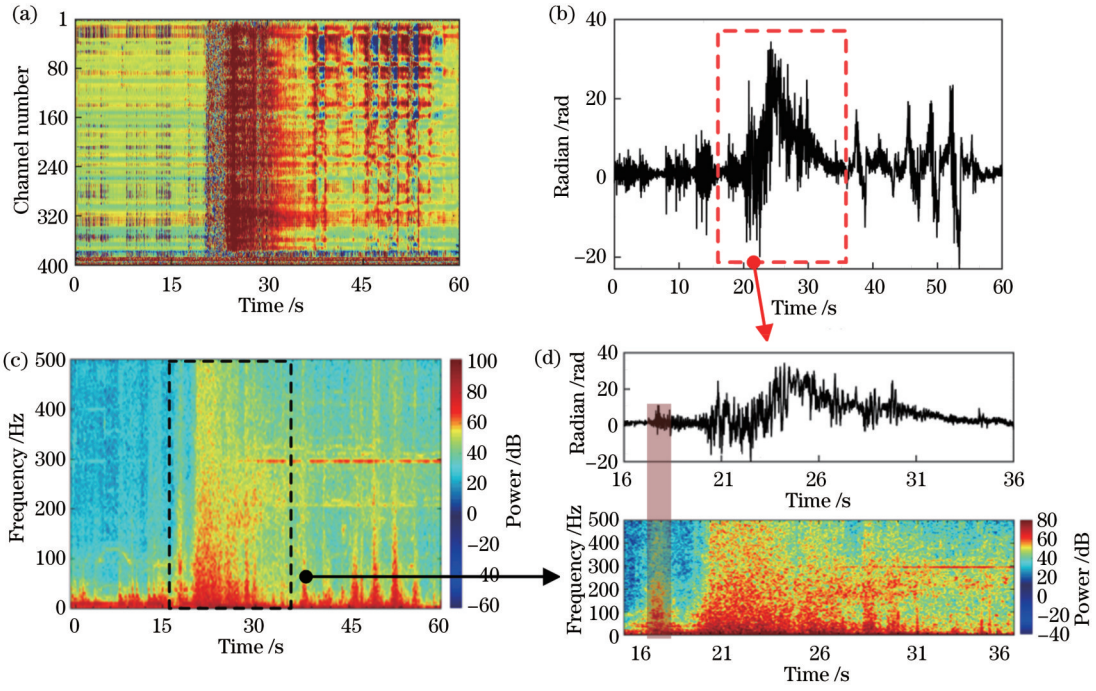

图5 基站入水的DAS记录。(a)2022年5月21日基站入水的60 s瀑布图；(b)第57道的单道振动数据；(c)第57道单道振动数据的时频谱；(d)第57道16～36 s的单道数据及其时频谱

Fig. 5 DAS records during base station entry. (a) Waterfall of 60 s long recording on May 21, 2022; (b) data of single channel vibration of 57th channel; (c) spectrogram of single channel vibration of 57th channel data; (d) data and spectrogram of single channel from 16 to 36 s of 57th channel

基站坐底过程会带来强大的冲击力，会对基站和海底地基的结构产生影响，在理想情况下基站应该以水平姿态坐底进行坐底。图6展示了基站着底时的DAS记录。图6(a)为单道时域记录，图6(b)为其时频谱。从图6(b)可以看出，基站着底时产生的振动频率主要集中在20 Hz以下。胡勇等[33]通过理论仿真得到深海潜水器以10°横倾角和艏部纵倾角姿态进行坐底过程中坐底单元的应力变化曲线，DAS实测数据对应的正则化能量谱与坐底单元应力变化曲线进行了对比[图6(c)]，发现实测信号出现了两个相邻的能量峰，

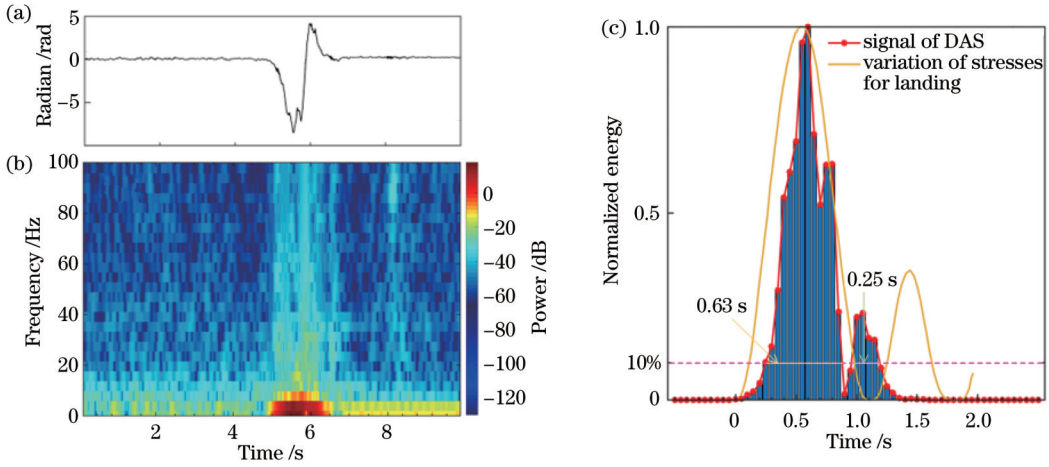

图6 基站着底的DAS记录。(a)基站着底的时域数据；(b)基站着底的DAS数据的时频谱；(c)基站着底的DAS数据的正则化能量谱与潜器坐底应力变化曲线对比。

Fig. 6 DAS records during base station landing. (a) Time series data of landing process; (b) time-frequency spectrogram of DAS data during base station landing; (c) comparison of normalized energy spectrum of DAS record of base station landing and stress variation curve during submersible's landing process

与应力变化曲线类似。第一个波峰从第0.2 s开始，在0.63 s内能量迅速降至10%以下，又一波峰紧接着出现，并持续0.25 s。DAS实测数据和理论曲线都表现出了相邻的两个峰，但实测振动信号的持续时间短于理论仿真曲线。此外，实测数据的第二个能量峰衰减比理论仿真的大，这说明着陆速度可能较低，或者基站在软质基底上着陆。需要注意的是，理论仿真的初始条件是深海潜水器以10°横倾角和艏部纵倾角姿态进行坐底，而实际情况下，基站的着陆过程可能保持了较好的水平状态，没有较大倾角。

图7记录了基站上浮时负载抛出的过程。从图7(a)可以看出，基站两侧负载分别释放时所产生的第一和第二个振动，两负载释放时间间隔约为3.8 s，此外还记录到了第二个释放负载与站体碰撞产生的第三个振动信号。图7(b)为对应的时频谱，三次振动的能量主要分布在60 Hz以下。以0.05 s为间隔进行频谱能量统计，获得各频率能量随时间的分布[见图7(c)与7(d)]，第一次抛载产生的能量主要分布在30 Hz以上，由于在第二次抛载时基站两侧配重不平衡，发生低频的整体晃动，所以20 Hz以下频段也分布了较高的能量。第二次负载释放与基站发生了意外碰撞，产生的振动信号主要在20 Hz以下。放大后时频谱见图7(e)，与三次振动的能量分布[见图7(d)]特征相符。

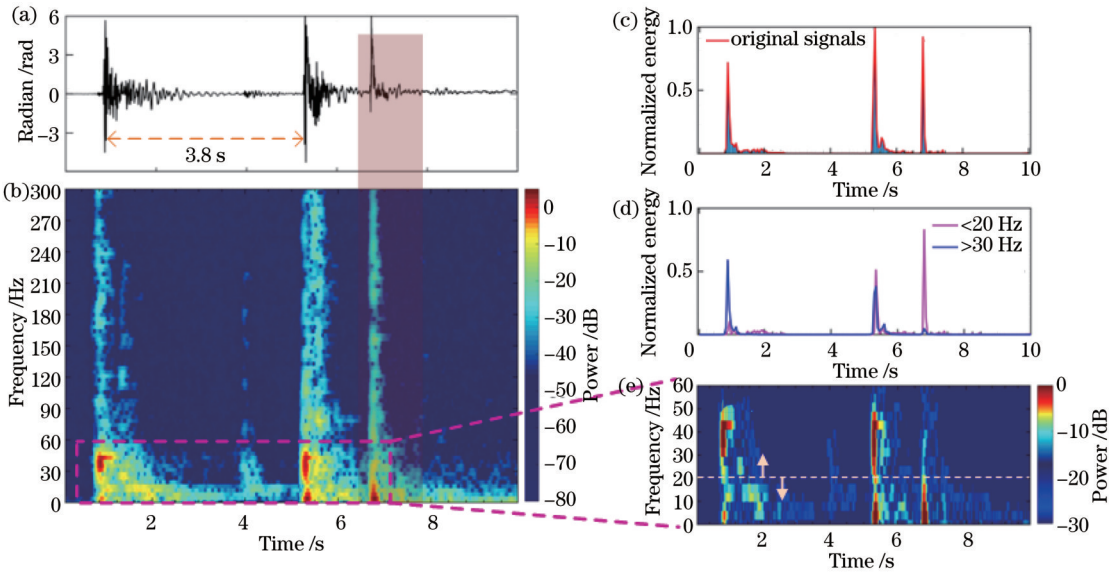

图7 基站抛载的DAS记录。(a) 基站抛载的时域数据；(b) 基站抛载的时频谱；(c) 未进行频率分割的原始信号的归一化能量的统计；(d) 经过频率分割的归一化能量统计；(e) 时频谱的放大图。

Fig. 7 DAS records of base station loads throwing. (a) Time series data of base station loads throwing; (b) time-frequency spectrum of base station loads throwing; (c) statistics of normalized energy of original signal without frequency segmentation; (d) statistics of normalized energy with frequency segmentation; (e) zoom in figure of time-frequency spectrum

基站通过舵式螺旋桨提供动力在海底实现位点转移，图8展示了基站位点转移任务的三种状态，分别是基站静止、螺旋桨调节以及基站移动。图8(a)为基站在静止状态下记录到的海洋背景噪声和设备运行的噪声。从时频谱上可以看出，36.3 Hz处的线谱能量较强，可能是基站上的设备固有谐振所引入的信号，并且在254 Hz处存在较明显的高次谐波。图8(b)展示了螺旋桨调节时的振动记录，23.2 Hz线谱应该对应螺旋桨低速运转时的基频振动，此外相比于静止状态，螺旋桨引入的振动谐波成分更加丰富。图8(c)为基站在运动状态下的DAS记录，振动信号幅度远高于前面两种状态，除了螺旋桨的振动信号引入的线谱外，还存在基站位移过程引入的海流冲击光缆导致的宽谱信号，两者叠加能量主要分布在60 Hz以下，但在95.9 Hz处有着非常强的干扰。图8(d)比较了上述三种状态的功率谱，可以看出，在基站不同状态下螺旋桨的出力不同导致其谐振频率不同，之前提到基站位移时的95.9 Hz强干扰应为基频16 Hz的高次谐波信号，此外即使在远离低频波段也体现出较强噪声，相比静止状态下噪声功率谱提高了7.37 dB以上。

4 结 论

DAS技术是一种近年兴起的高空间密度、长距离、动态测量的新型地震监测技术，其传感距离可达数十公里，道间距数米，结构简单，开发维护成本低，兼具实时数据传输功能，可有效降低观测成本，因此有望将这一全新技术应用在海洋关键区域。本文介绍了深海DAS系统的深海验证测试，在为期21天1423 m深的原位海试过程中，记录了超过600 GB的试验数据。对基站入水、着底、抛载以及移动过程中所产生的振动事件进行了分析，证明其具备深海作业能力以及振动信号探测能力，同时也验证了其深海环境运行的可靠性

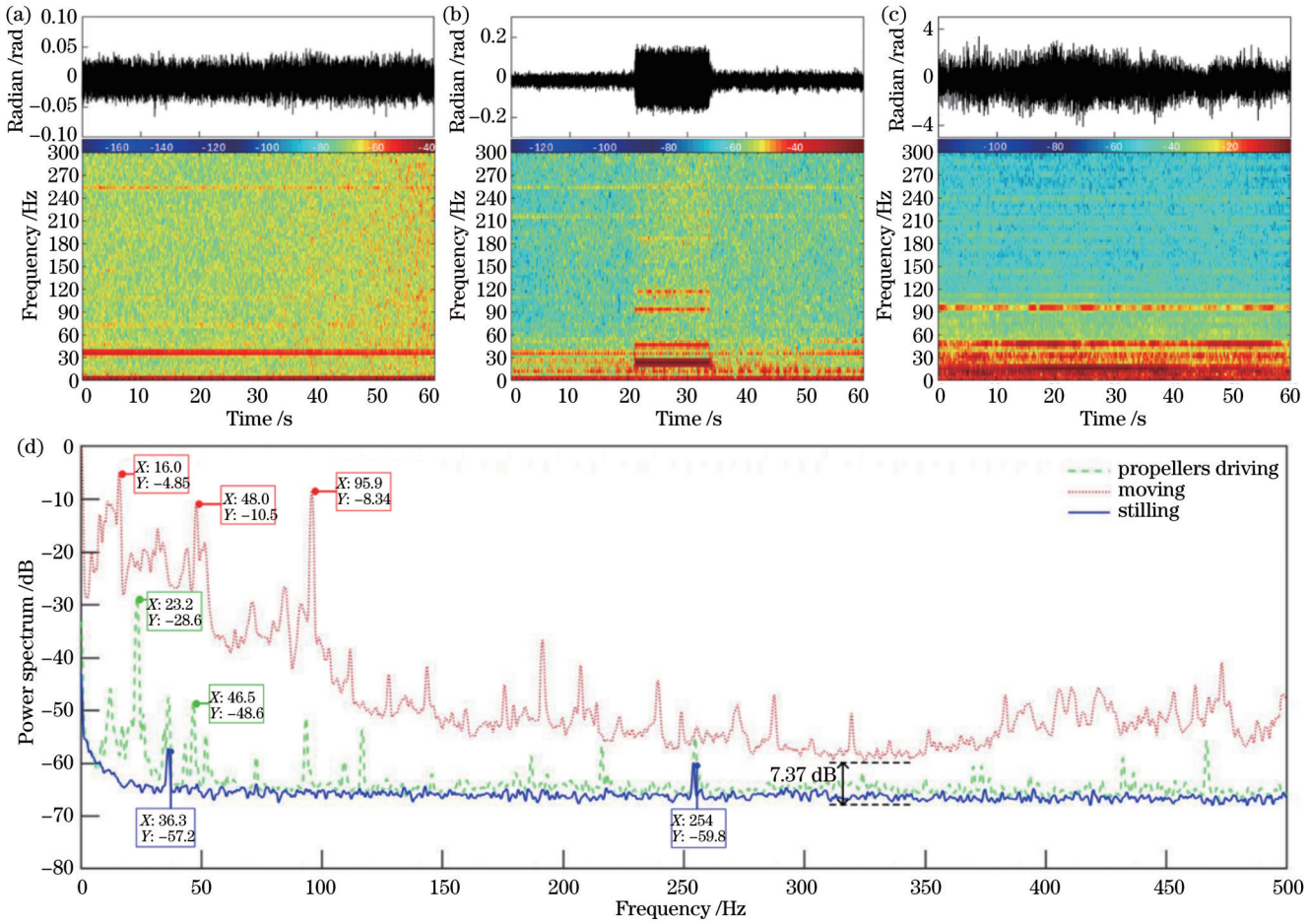

图 8 基站移动的 DAS 记录。(a) 基站静止的时域数据和时频谱;(b) 舵式螺旋桨姿态调整的时域数据和时频谱;(c) 基站移动的时域数据和时频谱;(d) 移动过程中的功率谱

Fig. 8 DAS records during base station moving. (a) Time series data and spectrogram of base station stilling; (b) time series data and spectrogram of rudder propellers′ gesture adjustment; (c) time series data and spectrogram of base station moving; (d) power spectrum of moving process

和稳定性,为后续深渊海试奠定了良好的基础。

参 考 文 献

[1] 司召鹏, 卜泽华, 毛邦宁, 等. 基于相位解调的相位敏感光时域反射计研究[J]. 激光与光电子学进展, 2022, 59(11): 1100007.
Si Z P, Bu Z H, Mao B N, et al. Review of research on phase sensitive optical time-domain reflectometer based on phase demodulation[J]. Laser & Optoelectronics Progress, 2022, 59(11): 1100007.

[2] 谢孔利, 饶云江, 冉曾令. 基于大功率超窄线宽单模光纤激光器的 Φ-光时域反射计光纤分布式传感系统[J]. 光学学报, 2008, 28(3): 569-572.
Xie K L, Rao Y J, Ran Z L. Distributed optical fiber sensing system based of Rayleigh scattering light Φ-OTDR using single-mode fiber laser with high power and narrow linewidth[J]. Acta Optica Sinica, 2008, 28(3): 569-572.

[3] Muanenda Y, Oton C J, Faralli S, et al. A cost-effective distributed acoustic sensor using a commercial off-the-shelf DFB laser and direct detection phase-OTDR[J]. IEEE Photonics Journal, 2015, 8(1): 6800210.

[4] Yuan Q, Wang F, Liu T, et al. Using an auxiliary Mach-Zehnder interferometer to compensate for the influence of laser-frequency-drift in Φ-OTDR[J]. IEEE Photonics Journal, 2018, 11(1): 7100209.

[5] Fernández-Ruiz M R, Martins H F, Pastor-Graells J, et al. Phase-sensitive OTDR probe pulse shapes robust against modulation-instability fading[J]. Optics Letters, 2016, 41(24): 5756-5759.

[6] Pastor-Graells J, Cortés L R, Martins H F, et al. 20 dB SNR enhancement in phase-sensitive OTDR using pulse stretching and recompression[J]. Proceedings of SPIE, 2017, 10323: 103230R.

[7] 张旭苹, 张益昕, 王峰, 等. 基于瑞利散射的超长距离分布式光纤传感技术[J]. 中国激光, 2016, 43(7): 0700002.
Zhang X P, Zhang Y X, Wang F, et al. Ultra-long fully distributed optical fiber sensor based on Rayleigh scattering effect [J]. Chinese Journal of Lasers, 2016, 43(7): 0700002.

[8] 王一凡, 刘庆文, 李赫, 等. 基于瑞利图形相关的光纤分布式动态应变传感器[J]. 中国激光, 2021, 48(11): 1110002.
Wang Y F, Liu Q W, Li H, et al. Distributed fiber-optic dynamic strain sensor based on spectra correlation of Rayleigh backscattering[J]. Chinese Journal of Lasers, 2021, 48(11): 1110002.

[9] 王杰, 贾新鸿, 饶云江, 等. 基于双向拉曼放大的相位敏感光时域反射仪[J]. 物理学报, 2013, 62(4): 044212.
Wang J, Jia X H, Rao Y J, et al. Phase-sensitive optical time-domain reflectometer based on bi-directional Raman amplification [J]. Acta Physica Sinica, 2013, 62(4): 044212.

[10] Peng Z P, Rao Y J, Peng F, et al. Long distance phase-sensitive optical time-domain reflectometer based on heterodyne detection and forward Raman amplification[J]. Journal of Optoelectronics Laser, 2014, 25(4): 724-729.

[11] Peng F, Wu H, Jia X H, et al. Ultra-long high-sensitivity Φ-OTDR for high spatial resolution intrusion detection of pipelines[J]. Optics Express, 2014, 22(11): 13804-13810.

[12] Li J, Wang Z N, Zhang L, et al. 124 km phase-sensitive OTDR with Brillouin amplification[J]. Proceedings of SPIE, 2014, 9157: 91575Z.

[13] Pan Z Q, Liang K Z, Ye Q, et al. Phase-sensitive OTDR system based on digital coherent detection[C]//2011 Asia Communications and Photonics Conference and Exhibition (ACP), November 13-16, 2011, Shanghai, China. New York: IEEE Press, 2012.

[14] Masoudi A, Belal M, Newson T P. A distributed optical fibre dynamic strain sensor based on phase-OTDR[J]. Measurement Science and Technology, 2013, 24(8): 085204.

[15] Fang G S, Xu T W, Feng S W, et al. Phase-sensitive optical time domain reflectometer based on phase-generated carrier algorithm[J]. Journal of Lightwave Technology, 2015, 33(13): 2811-2816.

[16] Feng S W, Xu T W, Huang J F, et al. Sub-meter spatial resolution phase-sensitive optical time-domain reflectometry system using double interferometers[J]. Applied Sciences, 2018, 8(10): 1899.

[17] Liang Y X, Wang Z N, Lin S T, et al. Optical-pulse-coding phase-sensitive OTDR with mismatched filtering[J]. Science China Information Sciences, 2022, 65(9): 192303.

[18] 杨震, 封皓. 基于深度学习的Φ-OTDR输油管道入侵监测研究[J]. 激光与光电子学进展, 2022, 59(8): 0806001.
Yang Z, Feng H. Oil pipeline intrusion monitoring based on deep learning of Φ-OTDR[J]. Laser & Optoelectronics Progress, 2022, 59(8): 0806001.

[19] 赵丽娟, 魏迎健, 徐志钮. 基于Φ-OTDR的振动事件识别分类器研究进展[J]. 光通信技术, 2023, 47(2): 1-5.
Zhao L J, Wei Y J, Xu Z N. Research progress of vibration event recognition classifier based on Φ-OTDR[J]. Optical Communication Technology, 2023, 47(2): 1-5.

[20] 李笑, 高毅, 吴昊, 等. 基于混合输入神经网络的Φ-OTDR系统模式识别方法[J]. 中国激光, 2023, 50(11): 1106003.
Li X, Gao Y, Wu H, et al. Mode recognition method of Φ-OTDR system based on mixed input neural network[J]. Chinese Journal of Lasers, 2023, 50(11): 1106003.

[21] Mestayer J, Cox B, Wills P, et al. Field trials of distributed acoustic sensing for geophysical monitoring[C]. SEG Technical Program Expanded Abstracts 2011. Houston: Society of Exploration Geophysicists, 2011: 4253-4257.

[22] Madsen K N, Thompson M, Parker T, et al. A VSP field trial using distributed acoustic sensing in a producing well in the North Sea[J]. First Break, 2013, 31(11): 3997.

[23] Lindsey N J, Dawe T C, Ajo-Franklin J B. Illuminating seafloor faults and sea dynamics with dark fiber distributed acoustic sensing[J]. Science, 2019, 366(6469): 1103-1107.

[24] Sladen A, Rivet D, Ampuero J P, et al. Distributed sensing of earthquakes and sea-solid Earth interactions on seafloor telecom cables[J]. Nature Communications, 2019, 10: 5777.

[25] Williams E F, Fernández-Ruiz M R, Magalhaes R, et al. Distributed sensing of microseisms and teleseisms with submarine dark fibers[J]. Nature Communications, 2019, 10: 5778.

[26] Spica Z J, Nishida K, Akuhara T, et al. Marine sediment characterized by sea-bottom fiber-optic seismology[J]. Geophysical Research Letters, 2020, 47(16): GL088360.

[27] Cheng F, Chi B X, Lindsey N J, et al. Utilizing distributed acoustic sensing and sea bottom fiber optic cables for submarine structural characterization[J]. Scientific Reports, 2021, 11: 5613.

[28] Williams E F, Fernández-Ruiz M R, Magalhaes R, et al. Scholte wave inversion and passive source imaging with sea-bottom DAS[J]. The Leading Edge, 2021, 40(8): 576-583.

[29] Matsumoto H, Araki E, Kimura T, et al. Detection of hydroacoustic signals on a fiber-optic submarine cable[J]. Scientific Reports, 2021, 11: 2797.

[30] Taweesintananon K, Landr M, Brenne J K, et al. Distributed acoustic sensing for near-surface imaging using submarine telecommunication cable: a case study in the Trondheimsfjord, Norway[J]. GEOPHYSICS, 2021, 86(5): B303-B320.

[31] Rivet D, de Cacqueray B, Sladen A, et al. Preliminary assessment of ship detection and trajectory evaluation using distributed acoustic sensing on an optical fiber telecom cable[J]. The Journal of the Acoustical Society of America, 2021, 149(4): 2615-2627.

[32] Bouffaut L, Taweesintananon K, Kriesell H J, et al. Eavesdropping at the speed of light: distributed acoustic sensing of baleen whales in the Arctic[J]. Frontiers in Marine Science, 2022, 9: 901348.

[33] 胡勇, 沈允生, 谢俊元, 等. 深海载人潜水器的坐底分析[J]. 船舶力学, 2008, 12(4): 642-648.
Hu Y, Shen Y S, Xie J Y, et al. Landing research on deep-sea Human Occupied Vehicle[J]. Journal of Ship Mechanics, 2008, 12(4): 642-648.

Field Trial of Deep-Sea Distributed Acoustic Sensing System in South China Sea

Deng Dimin[1], Xu Tuanwei[1,2*], Zhang Hanyu[3**], Yu Chunliang[4], Cao Kai[1,2], Jiang Yinghao[1,2], Xie Yaning[1,2], Li Fang[1,2], Wu Shiguo[3]

[1]*State Key Laboratory of Transducer Technology, Institute of Semiconductors, Chinese Academy of Sciences, Beijing* 100083, *China*;

[2]*College of Materials Science and Opto-Electronic Technology, University of Chinese Academy of Sciences, Beijing* 100049, *China*;

[3]*Laboratory of Marine Geophysics & Geo-Resources, Institute of Deep-Sea Science and Engineering, Chinese Academy of Sciences, Sanya* 572000, *Hainan*, *China*;

[4]*Deep-Sea Engineering Technology Department, Institute of Deep-Sea Science and Engineering, Chinese Academy of Sciences, Sanya* 572000, *Hainan*, *China*

Abstract

Objective Distributed acoustic sensing (DAS) technology regards the same optical fiber as both a sensing and transmission medium, enabling real-time capture of vibrations and acoustic signals in the vicinity of optical fibers. This technology features robust environmental adaptability, high sensitivity, and exceptional resistance to electromagnetic interference. DAS can transform optical cables spanning tens of kilometers into evenly distributed arrays for vibration and acoustic sensing, thus achieving spatial sampling resolutions of less than 1 m. Consequently, it has caught significant attention in fields such as oil and gas exploration and marine geophysics. However, the maximum sensing range of DAS is constrained by optical source bandwidth and stability, with the current maximum sensing range limited to approximately 100 km. Therefore, employing DAS for intercontinental undersea long-distance communication cables poses significant challenges. We introduce a DAS seabed *in-situ* monitoring system integrated with an underwater experiment platform, coupled with relevant offshore trials. This deployment extends DAS capabilities to more remote and deeper-sea areas. The analysis of offshore trial results validates the system feasibility. In the future, consideration can be given to combining submersible technologies for laying sensing optical cables on the seabed, which holds substantial significance for advancing marine geophysical research.

Methods We employ pressure chamber technology to construct a deep-sea DAS system capable of withstanding pressure at depths of up to 10000 m and conduct rigorous pressure testing in the laboratory, subjecting the system to pressure of up to 110 MPa. Subsequently, the system is deployed on a deep-sea *in-situ* experimental platform equipped with autonomous underwater mobility capabilities and is placed at a depth of 1423 m for *in-situ* testing. Throughout the sea trial, the base station undergoes various operational states including submersion, landing, moving, and raising, with distinct vibration data generated by each of these states. By analyzing the data collected by the DAS, we can discern the base station′s temporal and spectral characteristics in different operational conditions. These research findings confirm the feasibility of the design and deployment of deep-sea DAS systems in the extreme deep-sea environment.

Results and Discussions When the base station is stationary, DAS can capture the background noise of the sea, with an average noise level of $4.64\times10^{-4}\,\mathrm{rad}/\sqrt{\mathrm{Hz}}$, which closely aligns with laboratory measurements. The operational states of the base station can be primarily categorized as follows. ① When the base station submerges, there is a significant energy transfer upon contact with the seafloor, resulting in strong vibrations. Subsequently, the remaining modules of the base station enter the water one by one to generate a series of relatively weaker vibrations. ② When the base station lands on the seafloor, by comparing two consecutive impact signals, the energy of the second signal is observed to attenuate significantly compared to the first one, which indicates successful soft landing of the base station. ③ Before the base station is raised, the payload should be released. DAS records the produced vibration signals when the base station releases its payload. It is noticed that when the base station is in weight balance, the payload release primarily generates high-frequency signals above 30 Hz, but when it is not in balance, the signal energy is mainly distributed below 20 Hz. ④ When the base station moves underwater using servo propellers for direction control, compared to the stationary state, the rotation of the propellers and the movement of the base station introduce stronger interference below 60 Hz, and these interference signals′ harmonics are also present in the high-frequency range.

Conclusions DAS technology is a novel seismic monitoring technique emerging in recent years, and features high spatial

density, long-range capabilities, and dynamic measurements. Meanwhile, it offers sensing distances of up to several tens of kilometers with spatial resolution of a few meters. This technology is known for its simplicity, low development and maintenance costs, and ability to provide real-time data transmission, and it has the potential to significantly reduce observation costs, thus becoming a promising choice for deployment in critical marine regions. We present the deep-sea validation testing of the deep-sea DAS systems. During a 21-day *in-situ* sea trial at a depth of 1423 m, over 600 GB experimental data are recorded. Analysis of the vibration events generated during the base station′s submersion, settling on the seabed, payload release, and movement processes confirms its capability for deep-sea operations and vibration signal detection. Additionally, it validates the operational reliability and stability in the deep-sea environment, laying a strong foundation for future trials at depths of up to 10000 m.

Key words submarine distributed acoustic sensing system; distributed acoustic sensing; marine environmental monitoring; marine geophysics